University Faculty Publications and Creative Works

University Faculty Scholarship

1-1-2010

Brightest cluster galaxies and core gas density in rexcess clusters

Deborah B. Haarsma
Calvin University

Luke Leisman
Calvin University

Megan Donahue
Michigan State University

Seth Bruch
Michigan State University

Follow this and additional works at: https://digitalcommons.calvin.edu/calvin_facultypubs

Part of the Astrophysics and Astronomy Commons

Recommended Citation

BRIGHTEST CLUSTER GALAXIES AND CORE GAS DENSITY IN REXCESS CLUSTERS

DEBORAH B. HAARSMA[1], LUKE LEISMAN[1], MEGAN DONAHUE[2], SETH BRUCH[2], HANS BÖHRINGER[3], JUDITH H. CROSTON[4],
GABRIEL W. PRATT[3,5], G. MARK VOIT[2], MONIQUE ARNAUD[5], AND DANIELE PIERINI[3]
[1] Calvin College, 1734 Knollcrest SE, Grand Rapids, MI 49546, USA; dhaarsma@calvin.edu
[2] Physics and Astronomy, Michigan State University, East Lansing, MI 48824-2320, USA
[3] Max-Planck-Institut für extraterrestriche Physik, Giessenbachstraße, 85748 Garching, Germany
[4] School of Physics and Astronomy, University of Southampton, Southampton, SO17 1BJ, UK
[5] Laboratoire AIM, DAPNIA/Service d'Astrophysique, CEA/DSM, CNRS, Université Paris Diderot, Bât. 709, CEA-Saclay,
F-91191 Gif-sur-Yvette Cedex, France

ABSTRACT

We investigate the relationship between brightest cluster galaxies (BCGs) and their host clusters using a sample of nearby galaxy clusters from the Representative *XMM-Newton* Cluster Structure Survey. The sample was imaged with the Southern Observatory for Astrophysical Research in *R* band to investigate the mass of the old stellar population. Using a metric radius of $12\,h^{-1}$ kpc, we found that the BCG luminosity depends weakly on overall cluster mass as $L_{\rm BCG} \propto M_{\rm cl}^{0.18\pm0.07}$, consistent with previous work. We found that 90% of the BCGs are located within $0.035\,r_{500}$ of the peak of the X-ray emission, including all of the cool core (CC) clusters. We also found an unexpected correlation between the BCG metric luminosity and the core gas density for non-cool-core (non-CC) clusters, following a power law of $n_e \propto L_{\rm BCG}^{2.7\pm0.4}$ (where n_e is measured at $0.008\,r_{500}$). The correlation is not easily explained by star formation (which is weak in non-CC clusters) or overall cluster mass (which is not correlated with core gas density). The trend persists even when the BCG is not located near the peak of the X-ray emission, so proximity is not necessary. We suggest that, for non-CC clusters, this correlation implies that the same process that sets the central entropy of the cluster gas also determines the central stellar density of the BCG, and that this underlying physical process is likely to be mergers.

Key words: galaxies: clusters: general – galaxies: clusters: intracluster medium – galaxies: elliptical and lenticular, cD – X-rays: galaxies: clusters

Online-only material: color figures

1. INTRODUCTION

The intracluster gas in some galaxy clusters shows a central concentration in a cool core (CC). The higher density of this core gas allows more rapid energy loss in the form of X-ray emission. In the absence of other energy sources, the classic "cooling flow" model suggests that the central gas should cool. The cool gas would rapidly condense and form stars at rates greater than $100\,M_\odot$ yr^{-1}, but optical colors and spectral lines indicate much lower rates of less than $\sim 10\,M_\odot$ yr^{-1} (reviewed in Donahue & Voit 2004). Thus, the gas must be heated by other processes, such as active galactic nucleus (AGN) activity or other forms of feedback that regulate the thermal properties of the gas (reviewed in McNamara & Nulsen 2007). Yet the identity of the feedback process is still widely debated, and current simulations tend to overpredict the fraction of clusters with CCs (e.g., Kay et al. 2007).

The gas core is often located near the brightest cluster galaxy (BCG), particularly in CC clusters (Jones & Forman 1984; Bildfell et al. 2008; Rafferty et al. 2008; Sanderson et al. 2009). The BCG is not only luminous and massive, but has a more extended optical light profile than other ellipticals, due to its unique merger history at the bottom of the gravitational potential well (e.g., Hausman & Ostriker 1978; Vale & Ostriker 2008). Models predict that the BCG mass is correlated with the total cluster mass (e.g., De Lucia & Blaizot 2007), but the observed correlation is typically weaker (Lin & Mohr 2004; Popesso et al. 2007; Brough et al. 2008; Whiley et al. 2008; Yang et al. 2008; Mittal et al. 2009).

To better understand the connection between BCGs and CCs, we investigated the BCGs in 31 southern hemisphere clusters from the Representative *XMM-Newton* Cluster Structure Survey (REXCESS; Böhringer et al. 2007). The REXCESS sample was chosen to evenly represent the range of X-ray luminosities in the local ($0.06 < z < 0.18$) population, with no bias regarding X-ray morphology or central surface brightness. Thus, it provides an ideal laboratory for testing the connections between BCGs and their host clusters. Pratt et al. (2007), Croston et al. (2008), and Pratt et al. (2009) measure the X-ray luminosity, temperature, mass, core gas density, and cooling time. Here we present ground-based CCD (optical *R* band) imaging of the cluster BCGs and calculate colors relative to Two Micron All Sky Survey (2MASS) *K*-band magnitudes. We investigate the connections between the old stellar population and the properties of the X-ray gas.

Interestingly, the strongest correlation we found was not between the BCG mass and the total cluster mass, but between the central BCG stellar density and the core gas density. We describe the cluster sample and X-ray measurements in Section 2, and the *R*-band observations and BCG magnitude calculations in Section 3. In Sections 4 and 5, we examine this new correlation, as well as other connections between BCGs and their host clusters. Our conclusions are summarized in Section 6. We use $h = 0.7$, $\Omega_m = 0.3$, and $\Omega_\Lambda = 0.7$ throughout.

2. X-RAY SAMPLE

The REXCESS sample (Böhringer et al. 2007) contains 33 clusters selected to evenly sample a range of X-ray luminosities

Table 1
X-ray Properties

Cluster	Alt Name	z	r_{500} (kpc)	$n_e h(z)^{-2}$ (cm^{-3})	$\log(t_{\mathrm{cool}})$ (log(yr))	$\log(\langle w \rangle)$ (log(r_{500}))	$\log(M_{\mathrm{cl}})$ (log($M_\odot$))	X Peak Coordinates J2000	Offset (kpc)
(1)	(2)	(3)	(4)	(5)	(6)	(7)	(8)	(9)	(10)
RXCJ0003.8+0203	A2700	0.0924	876^{+5}_{-5}	0.0162 ± 0.0007	9.47 ± 0.02	-2.49 ± 0.12	$14.321^{+0.008}_{-0.008}$	00:03:49.7+02:03:58	5 ± 6
RXCJ0006.0−3443	A2721	0.1147	1059^{+10}_{-10}	0.0079 ± 0.0008	9.82 ± 0.02	-1.89 ± 0.05	$14.577^{+0.012}_{-0.013}$	00:05:59.9−34:43:23	14 ± 8
RXCJ0020.7−2542	A0022	0.1410	1045^{+5}_{-5}	0.0085 ± 0.0007	9.67 ± 0.02	-2.20 ± 0.05	$14.571^{+0.007}_{-0.007}$	00:20:42.2−25:42:25	32 ± 9
RXCJ0049.4−2931	S0084	0.1084	807^{+7}_{-7}	0.0182 ± 0.0014	9.37 ± 0.02	-2.64 ± 0.13	$14.221^{+0.012}_{-0.012}$	00:49:23.0−29:31:14	5 ± 7
RXCJ0145.0−5300	A2941	0.1168	1089^{+6}_{-6}	0.0038 ± 0.0005	9.92 ± 0.02	-1.52 ± 0.02	$14.614^{+0.008}_{-0.008}$	01:44:59.7−53:01:03	23 ± 8
RXCJ0211.4−4017	A2948	0.1008	685^{+3}_{-3}	0.0214 ± 0.0008	9.23 ± 0.02	-2.34 ± 0.09	$14.003^{+0.007}_{-0.007}$	02:11:24.8−40:17:28	1 ± 7
RXCJ0225.1−2928	. . .	0.0604	693^{+7}_{-8}	0.0038 ± 0.0005	9.60 ± 0.02	-1.92 ± 0.05	$14.003^{+0.014}_{-0.015}$	02:25:09.3−29:28:36	4 ± 4
RXCJ0345.7−4112	S0384	0.0603	688^{+5}_{-4}	0.0547 ± 0.0010	9.07 ± 0.02	-2.28 ± 0.07	$13.992^{+0.011}_{-0.008}$	03:45:46.2−41:12:14	4 ± 4
RXCJ0547.6−3152	A3364	0.1483	1133^{+5}_{-5}	0.0088 ± 0.0005	9.65 ± 0.02	-2.15 ± 0.03	$14.680^{+0.007}_{-0.007}$	05:47:38.4−31:52:12	39 ± 10
RXCJ0605.8−3518	A3378	0.1392	1045^{+5}_{-5}	0.0739 ± 0.0013	8.95 ± 0.02	-2.23 ± 0.03	$14.571^{+0.007}_{-0.007}$	06:05:54.2−35:18:09	7 ± 9
RXCJ0616.8−4748	. . .	0.1164	939^{+5}_{-6}	0.0119 ± 0.0006	9.64 ± 0.02	-1.88 ± 0.05	$14.421^{+0.008}_{-0.008}$	06:16:51.7−47:47:40	14 ± 8
RXCJ0645.4−5413	A3404	0.1644	1279^{+7}_{-7}	0.0245 ± 0.0014	9.37 ± 0.02	-2.41 ± 0.04	$14.846^{+0.008}_{-0.008}$	06:45:29.3−54:13:40	10 ± 11
RXCJ0821.8+0112	A0653	0.0822	755^{+6}_{-6}	0.0133 ± 0.0008	9.60 ± 0.02	-2.35 ± 0.12	$14.123^{+0.010}_{-0.011}$	08:21:50.9+01:11:52	6 ± 6
RXCJ0958.3−1103	A0907	0.1669	1077^{+18}_{-16}	0.0503 ± 0.0023	9.08 ± 0.02	-2.47 ± 0.08	$14.622^{+0.022}_{-0.020}$	09:58:22.3−11:03:54	17 ± 11
RXCJ1044.5−0704	A1084	0.1342	931^{+2}_{-2}	0.1015 ± 0.0018	8.87 ± 0.02	-2.14 ± 0.02	$14.419^{+0.004}_{-0.004}$	10:44:33.0−07:04:09	4 ± 9
RXCJ1141.4−1216	A1348	0.1195	885^{+3}_{-2}	0.0701 ± 0.0010	8.94 ± 0.02	-2.27 ± 0.05	$14.345^{+0.004}_{-0.004}$	11:41:24.4−12:16:37	5 ± 8
RXCJ1236.7−3354	A0700	0.0796	753^{+6}_{-0}	0.0125 ± 0.0007	9.41 ± 0.02	-2.28 ± 0.05	$14.118^{+0.011}_{-0.002}$	12:36:41.3−33:55:37	8 ± 6
RXCJ1302.8−0230	A1663	0.0847	842^{+4}_{-4}	0.0347 ± 0.0006	9.20 ± 0.02	-1.82 ± 0.02	$14.265^{+0.007}_{-0.007}$	13:02:53.3−02:31:00	17 ± 6
RXCJ1311.4−0120	A1689	0.1832	1319^{+4}_{-4}	0.0465 ± 0.0011	9.16 ± 0.02	-2.40 ± 0.03	$14.893^{+0.004}_{-0.004}$	13:11:29.5−01:20:28	1 ± 12
RXCJ1516.3+0005	A2050	0.1181	989^{+3}_{-3}	0.0109 ± 0.0006	9.61 ± 0.02	-2.43 ± 0.05	$14.490^{+0.005}_{-0.005}$	15:16:18.1+00:05:28	16 ± 8
RXCJ1516.5−0056	A2051	0.1198	927^{+6}_{-5}	0.0104 ± 0.0008	9.66 ± 0.02	-1.75 ± 0.03	$14.405^{+0.009}_{-0.008}$	15:16:44.2−00:58:12	6 ± 8
RXCJ2014.8−2430	. . .	0.1538	1155^{+4}_{-4}	0.1291 ± 0.0023	8.74 ± 0.02	-2.24 ± 0.02	$14.707^{+0.005}_{-0.005}$	20:14:51.7−24:30:20	5 ± 10
RXCJ2023.0−2056	S0868	0.0564	739^{+6}_{-6}	0.0092 ± 0.0009	9.61 ± 0.02	-1.78 ± 0.04	$14.084^{+0.011}_{-0.011}$	20:22:58.8−20:56:56	4 ± 4
RXCJ2129.8−5048	A3771	0.0796	900^{+7}_{-8}	0.0052 ± 0.0005	9.91 ± 0.02	-1.38 ± 0.17	$14.351^{+0.011}_{-0.012}$	21:29:40.9−50:48:55	51 ± 6
RXCJ2149.1−3041	A3814	0.1184	886^{+4}_{-4}	0.0549 ± 0.0011	8.92 ± 0.02	-2.47 ± 0.06	$14.347^{+0.006}_{-0.006}$	21:49:07.6−30:42:05	4 ± 8
RXCJ2157.4−0747	A2399	0.0579	751^{+4}_{-4}	0.0034 ± 0.0003	10.02 ± 0.02	-0.97 ± 0.97	$14.106^{+0.009}_{-0.009}$	21:57:29.5−07:47:55	12 ± 4
RXCJ2217.7−3543	A3854	0.1486	1022^{+4}_{-4}	0.0182 ± 0.0009	9.45 ± 0.02	-2.74 ± 0.49	$14.546^{+0.006}_{-0.006}$	22:17:45.5−35:43:30	10 ± 10
RXCJ2218.6−3853	A3856	0.1411	1130^{+7}_{-8}	0.0126 ± 0.0010	9.50 ± 0.02	-1.81 ± 0.01	$14.673^{+0.009}_{-0.009}$	22:18:40.3−38:54:06	29 ± 9
RXCJ2234.5−3744	A3888	0.1510	1283^{+4}_{-5}	0.0063 ± 0.0005	9.80 ± 0.02	-2.12 ± 0.03	$14.843^{+0.005}_{-0.005}$	22:34:27.1−37:44:02	112 ± 10
RXCJ2319.6−7313	A3992	0.0984	788^{+5}_{-5}	0.0571 ± 0.0018	8.80 ± 0.02	-1.66 ± 0.02	$14.186^{+0.009}_{-0.009}$	23:19:40.2−73:13:38	5 ± 7

Notes. (1) Name of cluster in REXCESS catalog. (2) Alternate name of the cluster. (3) Redshift of the cluster. (4) The radius of the cluster enclosing a mean overdensity of 500 times the critical density, found by Croston et al. (2008) using the $M_{500} - Y_X$ relation of Arnaud et al. (2007). (5) Gas density at 0.008 r_{500}, from Croston et al. (2008). (6) Gas cooling time at 0.03 r_{500}, from Croston et al. (2008); we classify CCs as $t_{\mathrm{cool}} < 2 \times 10^9$ yr or $\log(t_{\mathrm{cool}}) < 9.3$. (7) Standard deviation of centroid shifts, from Böhringer et al. (2009); we classify disturbed clusters as $\langle w \rangle > 0.01$ r_{500}. (8) Total cluster mass, found by Pratt et al. (2009) using the $M_{500} - Y_X$ relation of Arnaud et al. (2007). (9) Coordinates of the peak of the X-ray emission, from Böhringer et al. (2009), with an uncertainty of 4″. (10) Offset of the selected BCG from the peak X-ray position.

and temperatures (2–9 keV), including a variety of dynamical states and core cooling times.

Croston et al. (2008) derived the radial gas density profiles for the REXCESS sample from *XMM-Newton* surface brightness profiles, using a non-parametric deprojection and PSF-deconvolution method. Croston et al. (2006) showed that this method accurately recovers the gas density profile observed in higher resolution *Chandra* data, down to 2″.4 radius, for data of similar statistical quality to REXCESS. Two clusters, RXCJ0956 and RXCJ2152, were excluded from the X-ray analysis because they have multiple distinct components which preclude a one-dimensional profile analysis, leaving a sample of 31 clusters.

Relevant X-ray properties are listed in Table 1. The scaling radius r_{500} (defined as the radius enclosing a mean overdensity of 500 times the critical density) and the corresponding cluster mass M_{cl} was found from iterations about the $M_{500} - Y_X$ relation

of Arnaud et al. (2007). The cooling time was determined at a radius of 0.03 r_{500} (about 10″–20″). The core gas density n_e was measured at a radius of 0.008 r_{500} (about 3″–6″) and was scaled by $h(z)^{-2}$ to remove evolution effects. The dynamical state of the gas was characterized by $\langle w \rangle$, the standard deviation of the offsets w between the X-ray peak and the centroids of emission found for various radii (Böhringer et al. 2009). Pratt et al. (2009) identified a subsample of REXCESS as CC clusters using a cutoff in core gas density. We chose instead to use a cutoff in cooling time (at 0.03 r_{500}), since the cooling time can be compared to various dynamical time scales in the cluster. We defined CC clusters to be those with $t_{\mathrm{cool}} < 2$ Gyr ($\log t_{\mathrm{cool}} < 9.3$), marked with blue stars on the figures. Non-cool-core (non-CC) clusters have $t_{\mathrm{cool}} > 2$ Gyr. Compared to Pratt et al. (2009), this definition shifts only one cluster into the CC sample, namely RXCJ0211; see Section 5.

Table 2
Observations

Date	Targets	Telescope Instrument
2007 Sep 15	RXCJ 2217, 2218, 2234, 2319	SOAR SOI
2007 Oct 11	RXCJ 0345, 0547, 0605, 0645	SOAR SOI
2008 Mar 8	RXCJ 0821, 0958, 1516.3, 1516.5	SOAR SOI
2008 Jul 6	RXCJ 2014, 2023, 2048, 2129, 2157	SOAR SOI
2008 Jul 7	RXCJ 0006, 0020, 0049, 0145, 0211, 0225	SOAR SOI
2008 Oct 4	RXCJ 2149	SOAR Goodman
2008 Nov 2	RXCJ 0003	SOAR Goodman
2009 Jan 15–16	RXCJ 1044	Lowell Hall 42″
2009 Apr 17	RXCJ 0616, 1141	SOAR Goodman
2009 Apr 27	RXCJ 1236, 1302	SOAR Goodman
…	RXCJ 1311	SDSS

Pratt et al. (2009) also identified clusters as morphologically disturbed if $\langle w \rangle > 0.01 r_{500}$. We use the same cut-off but with revised values of $\langle w \rangle$ from Böhringer et al. (2009). Disturbed clusters are marked with red squares on the figures. In these clusters the gas distribution is less symmetric, likely due to a recent merger of sub-clusters and a younger dynamical age. In general, disturbed clusters do not have CCs (although RXCJ1302 and RXCJ2319 are exceptions).

For each cluster, the position of the X-ray peak emission has been determined by Böhringer et al. (2009), who describe the method in detail. Briefly, the peak position for most clusters is the local maximum in a 4″ smoothed image. In a few clusters the central surface brightness is flat, so the peak position is given as the center of a dipole fitted at 0.1 r_{500}. The positions were confirmed by visual inspection. These positions are more precise and accurate than the low-resolution *ROSAT* positions listed in Böhringer et al. (2007).

3. OPTICAL DATA

3.1. Observations

Table 2 lists our observations, which, with the exception of two targets, were made with the 4.1 m Southern Observatory for Astrophysical Research (SOAR) in Cerro Pachón, Chile. Most of the SOAR observations used the SOAR Optical Imager (SOI; Walker et al. 2003; Schwarz et al. 2004), consisting of two thinned, back-illuminated 4096 × 4096 CCDs. The field of view is over 5′ across, with a binned pixel size of 0″.154 from a natural pixel size of 0″.0767. The standard observing strategy was three 200 s exposures, dithered by 10″ to span the gap between the two CCDs. The remaining SOAR observations used the Goodman Spectrograph (Clemens et al. 2004) in imaging mode, which utilizes a single Fairchild CCD. The field of view is 7′.2 in diameter, with a binned pixel size of 0″.29 from a natural pixel size of 0″.15. The standard observing strategy was a single 600 s exposure. One target (RXCJ1044) was observed at the 42 inch (1.1 m) John S. Hall Telescope at Lowell Observatory in New Mexico, using a 2048 × 2048 CCD camera with pixel size 0″.59; we made 15 dithered exposures of 600 s each. All observations were made under clear photometric conditions; if the conditions or data were suspect in any way, the galaxy was reobserved. The seeing was typically 1″. Finally, one target (RXCJ1311) was mistakenly omitted from observations but is one of the few to appear in the Sloan Digital Sky Survey (SDSS; Adelman-McCarthy et al. 2008). SDSS data have sufficient resolution (pixel size 0″.396) and depth for our measurements; a Luminous Red Galaxy spectral template was used to transform the r' data to the Cousins R filter (center ∼630 nm) that we used for all other observations.

The images were reduced in the standard fashion using IRAF[6] v.2.12.2, including bias subtraction, flat field correction, and cosmic ray removal. The dithered images were aligned and median combined for each target, compensating for differing background levels if necessary. The background value of the combined image was measured using APPHOT in a 1–2 arcmin radius annulus centered on the BCG with the radius chosen to avoid field objects. The data were corrected for air mass assuming an R-band extinction coefficient of −0.1, and calibrated to the Vega magnitude scale using Landolt (1992) standard stars or Hamuy et al. (1992) spectrophotometric standard stars. The data were converted to the AB scale with $R_{AB} = R_{vega} + 0.206$; all magnitudes and colors are reported on the AB scale.

The uncertainty in the final magnitudes is dominated by systematics. Because the BCGs are bright and cover many pixels, the random error on the summed flux and on the subtracted background is much smaller than the total systematic error in the flat-field corrections, standard star calibration, air-mass corrections, and variation in sky conditions throughout the night. We estimate the uncertainty due to these systematics to be around 0.05 mag and assume this value for all observations.

Images of a select subsample of the BCGs are shown in Figure 1. The entire sample is available at http://www.calvin.edu/~dhaarsma/rexcess. The optical images are overlaid with contours of the *XMM-Newton* data, taken in the 0.5–2 keV band with all three detectors combined. The X-ray surface brightness images were corrected for vignetting and detector gaps, point sources were removed and smoothly refilled, and the images were smoothed with a 4″ Gaussian.

3.2. Surface Brightness Profiles

Figure 2 shows the observed surface brightness profiles of the BCGs, corrected for Galactic extinction, to rest frame, and for cosmological surface brightness dimming. The slopes appear similar across the sample.

Postman & Lauer (1995) characterized the profile using the slope of the integrated profile, $\alpha = d \log (L_r)/d \log(r)$. They found that α depends on metric luminosity, and that this dependence could be removed to improve the utility of BCGs as standard candles. We measured α for this sample and found no correlation with metric luminosity, as well as an absence of low α values. This confirms the work of P. Lyman discussed in Böhringer et al. (2001).

We also fit de Vaucouleurs functions to the profiles, but again found no correlation between profile shape (r_{eff}) and metric luminosity. (A typical de Vaucouleurs function is plotted in Figure 2.) Instead, we found the metric luminosity to be correlated with surface brightness at a given metric radius (the vertical offset in Figure 2). Thus, these BCGs share the same profile shape but differ in their overall brightness.

3.3. BCG Identification

Tables 3 and 4 list the optical properties of the BCGs. We classified the clusters into three categories. (1) Clusters where a central galaxy is clearly the brightest and has a generally smooth light distribution. (2) Clusters where a central galaxy is clearly the brightest, but has multiple light peaks appearing in the BCG envelope. These may be stars, foreground galaxies, infalling galaxies on a radial path, member galaxies in low radius orbits,
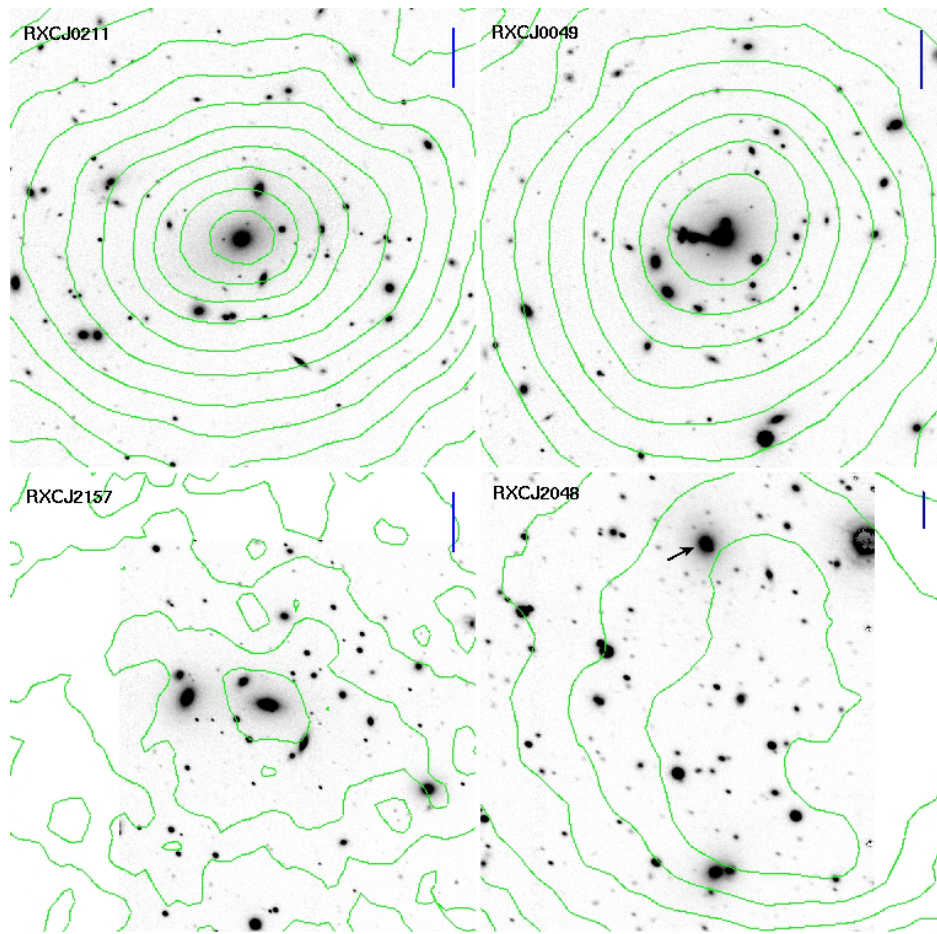
Figure 1. Images of REXCESS BCGs. The complete sample can be viewed at http://www.calvin.edu/~dhaarsma/rexcess/. The four clusters shown here illustrate our classification scheme: RXCJ0211 is type 1 (brightest, smooth), RXCJ0049 is type 2 (brightest, lumpy), RXCJ2157 is type 3 (multiple galaxies of similar brightness) with the X-ray peak clearly selecting one galaxy, and RXCJ2048 is type 3 with the X-ray peak far from any galaxy. North is up and east left. Gray scale: *R* band. Vertical bar: 50 kpc at redshift of the cluster. Contours: X-ray surface brightness from *XMM-Newton*, 0.5–2 keV, with contours increasing in steps of $\sqrt{2}$.

(A color version of this figure is available in the online journal.)

or mergers in progress. (3) Clusters in which there are two or more galaxies of similar brightness. Figure 1 includes examples of each type.

We identified the BCG using aperture magnitudes, with two borderline cases decided by proximity to other galaxies or to the X-ray peak. The fields were inspected visually in the Digital Sky Survey out to $500\,h^{-1}$ kpc; if there was any ambiguity about the brightest galaxy or the X-ray peak position, the $5'$–$7'$ field of view was positioned to cover other candidates. The brightness was measured for galaxies within this field of view (typically a $200\,h^{-1}$ kpc radius around the X-ray peak). We used an unmasked $50\,h^{-1}$ kpc aperture in order to include light from the extended envelope and mergers in progress. One borderline case was RXCJ2234, in which three galaxies had nearly the same brightness (within 0.01 mag) and none were near the X-ray peak, so we choose the one located in the middle of the group. The other case is RXCJ1311 (Abell1689), in which some galaxies had a neighbor galaxy within the $50\,h^{-1}$ kpc aperture which boosted their brightness; measurements in a smaller ($12\,h^{-1}$ kpc) unmasked aperture identified two galaxies with similar brightness (within 0.06 mag) near the center of the group, so we choose the one located at the X-ray peak.

BCGs located more than $0.03\ r_{500}$ from the X-ray peak are marked with an arrow in Figure 1, and with a green X in Figures 3–8. Table 4 lists the 2MASS identification of the
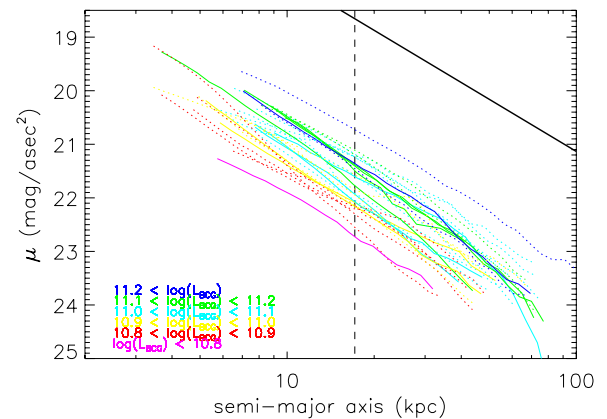

Figure 2. *R*-band surface brightness profiles of the BCGs, including *k*-corrections, extinction corrections, and corrections for surface brightness dimming. The data are plotted only for radii greater than 3 arcsec and less than twice the isophotal radius (isophote of 22.5 mag arcsec^{-2}). Solid lines are the CC population, dotted lines are the remaining BCGs. The vertical dashed line indicates the metric radius of $12\,h^{-1}$ kpc. The thick line in the upper right indicates the shape of a typical de Vaucouleurs profile (effective radius of 60 kpc). In the online version of the paper, the colors of the lines indicate the metric luminosity of the BCG, showing the correlation with the surface brightness at the metric radius.

(A color version of this figure is available in the online journal.)

Table 3
Optical Properties: Metric

BCG coord J2000	R_{met} (mag)	$R_{met,abs}$		L_{BCG} (log($L_\odot$))	PA (deg)	e	μ (mag arcsec^{-1})
		Observed	Rest Frame				
(1)	(2)	(3)	(4)	(5)	(6)	(7)	(8)
00:03:49.6+02:04:00	15.06	−23.07	−23.16	11.06 ± 0.02	−81	0.45	21.24
00:05:59.6−34:43:17	15.59	−23.04	−23.16	11.06 ± 0.02	−77	0.51	21.18
00:20:43.1−25:42:28	16.23	−22.89	−23.04	11.01 ± 0.02	24	0.47	21.22
00:49:22.8−29:31:12	15.53	−22.98	−23.09	11.03 ± 0.02	−25	0.04	21.92
01:44:58.9−53:01:12	16.22	−22.46	−22.58	10.83 ± 0.02	74	0.21	22.15
02:11:24.8−40:17:28	15.64	−22.70	−22.80	10.91 ± 0.02	−62	0.23	22.09
02:25:09.0−29:28:38	14.61	−22.55	−22.61	10.84 ± 0.02	−76	0.31	22.16
03:45:46.0−41:12:16	13.87	−23.28	−23.34	11.13 ± 0.02	52	0.09	21.77
05:47:37.7−31:52:24	16.36	−22.88	−23.05	11.01 ± 0.02	19	0.09	22.05
06:05:53.9−35:18:08	16.08	−23.01	−23.16	11.06 ± 0.02	−73	0.11	21.93
06:16:51.7−47:47:45	15.22	−23.45	−23.57	11.22 ± 0.02	83	0.53	20.73
06:45:29.5−54:13:37	16.26	−23.23	−23.41	11.16 ± 0.02	65	0.31	21.19
08:21:50.7+01:11:49	15.21	−22.66	−22.74	10.89 ± 0.02	−18	0.34	22.30
09:58:22.0−11:03:51	16.56	−22.96	−23.14	11.05 ± 0.02	−27	0.26	21.60
10:44:32.9−07:04:07	16.39	−22.62	−22.76	10.90 ± 0.02	2	0.29	22.07
11:41:24.2−12:16:37	15.49	−23.24	−23.37	11.14 ± 0.02	−7	0.27	21.40
12:36:41.3−33:55:32	14.91	−22.87	−22.95	10.97 ± 0.02	−16	0.13	22.14
13:02:52.6−02:30:59	15.15	−22.78	−22.86	10.94 ± 0.02	78	0.22	22.16
13:11:29.5−01:20:28	16.63	−23.11	−23.31	11.12 ± 0.02	58	0.13	21.49
15:16:17.9+00:05:21	15.87	−22.83	−22.95	10.98 ± 0.02	43	0.41	21.57
15:16:44.2−00:58:09	15.80	−22.94	−23.06	11.02 ± 0.02	−45	0.29	21.59
20:14:51.7−24:30:22	16.10	−23.33	−23.51	11.20 ± 0.02	37	0.21	21.38
20:22:59.1−20:56:56	14.14	−22.86	−22.91	10.96 ± 0.02	−66	0.09	21.95
20:48:11.6−17:49:03	15.83	−23.40	−23.56	11.22 ± 0.02	16	0.14	21.45
21:29:42.4−50:49:26	15.10	−22.69	−22.76	10.90 ± 0.02	10	0.19	22.20
21:49:07.4−30:42:05	15.29	−23.42	−23.55	11.21 ± 0.02	0	0.19	21.36
21:57:29.4−07:47:44	14.45	−22.61	−22.67	10.86 ± 0.02	80	0.42	22.55
22:17:45.8−35:43:29	16.00	−23.25	−23.41	11.16 ± 0.02	−22	0.20	21.11
22:18:39.4−38:54:02	16.03	−23.09	−23.24	11.09 ± 0.02	−35	0.36	21.24
22:34:24.6−37:43:31	16.47	−22.81	−22.98	10.98 ± 0.02	18	0.15	21.84
23:19:40.5−73:13:36	16.39	−21.88	−21.99	10.59 ± 0.02	0	0.26	22.72

Notes. All magnitudes and colors are on the AB scale and corrected for Galactic dust extinction. (1) BCG coordinates. (2) R-band apparent magnitude in metric radius of $12\,h^{-1}$ kpc, uncertainty of 0.05 mag. (3) and (4) R band absolute magnitude in metric radius of $12\,h^{-1}$ kpc, uncertainty of 0.05 mag. Column 4 is converted to rest frame. (5) Luminosity of BCG corresponding to $R_{met,abs}$ converted to rest frame. (6)–(8) Position angle (degrees E of N), ellipticity, and corrected surface brightness of the isophote with semi-major axis $12\,h^{-1}$ kpc.

galaxy, but we were able to better resolve the crowded fields and determine a more accurate position of the BCG center, which we list in Table 3.

3.4. Integrated Magnitudes

Because of the crowded fields around BCGs, a simple aperture magnitude would be biased by extra flux from other galaxies in the field. Instead, we masked light from sources unrelated to the BCG, then fit elliptical isophotes to the remaining light distribution using the IRAF task ELLIPSE. We then integrated the isophotes numerically to get the total flux.

Masked objects included stars, foreground galaxies, and cluster members not physically near the BCG. Some of the brightness peaks in the envelope, however, are the cores of cluster members in the process of merging with the BCG (such multiple nuclei are particularly visible in BCGs we classify as type 2). One approach would be to include the light from all objects that are already merging in the envelope. That is difficult, however, to implement, because it would require discriminating between foreground galaxies and galaxies physically near the BCG, and determining a priori how much a galaxy must be apparently assimilated in order to include it with the BCG light. We chose instead to mask all brightness peaks except the BCG center, and to fit isophotes only to light in a smooth elliptical distribution around that center. This procedure provides a consistent measure without subjective decisions on which brightness peaks to include. As a test, we measured the magnitudes in a $50\,h^{-1}$ kpc radius aperture without any masking, and found that the standard deviation of the absolute magnitudes increased from 0.29 to 0.34 mag; thus, the small masked aperture is a more consistent measure.

When fitting ellipses, we fixed the central coordinates but allowed the ellipticity and position angle to vary with radius. If the ellipticity or position angle changed rapidly or the fit failed due to too much masking, we adjusted the masks to achieve a smooth fit. To prevent double counting we discarded any overlapping isophotes.

The fitted isophotes were then integrated numerically, effectively replacing flux in the masked areas. During integration, we simulated a circular metric aperture by calculating the fraction of each ellipse inside the circular aperture. The apparent metric magnitude in a radius of $12\,h^{-1}$ kpc (17 kpc for our assumed cosmology, about $5''$–$15''$) is listed in Table 3 as R_{met}.

The apparent magnitude was converted to an absolute magnitude using the known redshifts. We applied the Galactic

Table 4
Optical Properties: Isophotal

| 2MASS Name | Class | Aper (″) | R_{K20} (mag) | $R - K$ color | | $J - K$ color Rest Frame | SMA (kpc) |
| | | | | Observed | Rest Frame | | |
(1)	(2)	(3)	(4)	(5)	(6)	(7)	(8)
2MASX J00034964+0203594	1	20.2	14.57	1.31	1.08 ± 0.10	0.18 ± 0.10	40
2MASX J00055975−3443171	1	12.4	15.46	1.18	0.90 ± 0.10	−0.05 ± 0.10	41
2MASX J00204314−2542284	2	18.7	15.32	1.39	1.01 ± 0.09	0.14 ± 0.09	47
2MASS J00492286−2931124	2	...	...	...	...	...	30
2MASX J01445891−5301110	3	10.6	16.01	1.17	0.88 ± 0.13	0.15 ± 0.16	25
2MASX J02112484−4017261	1	15.3	15.33	1.23	0.98 ± 0.11	−0.03 ± 0.12	28
2MASS J02250904−2928383	3	...	...	...	...	...	29
2MASX J03454640−4112149	1	22.3	13.61	1.18	1.03 ± 0.07	0.08 ± 0.06	28
2MASX J05473773−3152237	1	11.5	16.00	1.34	0.94 ± 0.16	0.11 ± 0.18	26
2MASX J06055401−3518081	1	9.8	15.87	1.44	1.07 ± 0.09	0.21 ± 0.11	25
2MASX J06165166−4747434	1	18.0	14.74	1.16	0.87 ± 0.10	0.04 ± 0.11	65
2MASX J06452948−5413365	1	14.7	15.73	1.33	0.87 ± 0.13	0.13 ± 0.15	39
2MASX J08215065+0111495	1	12.9	15.06	1.22	1.02 ± 0.11	0.10 ± 0.12	21
2MASX J09582201−1103500	1	11.3	16.03	1.56	1.10 ± 0.12	0.13 ± 0.13	40
2MASX J10443287−0704074	1	7.1	16.49	1.26	0.90 ± 0.12	0.04 ± 0.13	25
2MASX J11412420−1216386	1	11.2	15.37	1.34	1.03 ± 0.09	0.16 ± 0.09	38
2MASX J12364125−3355321	1	16.1	14.62	0.90	0.71 ± 0.09	−0.06 ± 0.09	23
2MASX J13025254−0230590	1	14.4	14.97	1.61	1.40 ± 0.09	0.13 ± 0.08	24
2MASX J13112952−0120280	1	8.2	16.32	1.48	0.96 ± 0.12	0.13 ± 0.13	26
2MASX J15161794+0005203	1	10.1	15.76	1.36	1.05 ± 0.11	0.14 ± 0.12	34
2MASX J15164416−0058096	1	11.6	15.60	1.17	0.86 ± 0.11	0.02 ± 0.12	33
2MASX J20145171−2430229	1	9.4	15.84	1.28	0.86 ± 0.10	0.06 ± 0.11	36
2MASX J20225911−2056561	2	19.9	13.77	0.79	0.65 ± 0.09	−0.09 ± 0.08	25
2MASX J20481162−1749034	3	9.3	15.63	1.27	0.87 ± 0.10	0.01 ± 0.11	36
2MASX J21294244−5049260	3	11.6	15.27	1.03	0.84 ± 0.10	−0.08 ± 0.11	25
2MASX J21490737−3042043	1	14.0	14.91	1.12	0.81 ± 0.09	0.04 ± 0.08	38
2MASX J21572939−0747443	3	10.3	14.72	1.13	0.99 ± 0.07	0.01 ± 0.06	18
2MASX J22174585−3543293	1	13.6	15.25	1.32	0.91 ± 0.10	0.09 ± 0.11	45
2MASX J22183938−3854018	2	14.1	15.50	1.23	0.85 ± 0.09	0.08 ± 0.09	51
2MASX J22342463−3743304	3	11.0	15.88	1.24	0.83 ± 0.10	0.00 ± 0.11	33
2MASX J23194046−7313366	1	9.7	16.44	1.54	1.30 ± 0.13	0.43 ± 0.17	16

Notes. All magnitudes and colors (including 2MASS) are on the AB scale and corrected for Galactic dust extinction. (1) 2MASS name of selected BCG (see Section 5 for RXCJ0049 and RXCJ0225). (2) BCG classification (see Section 3.3. (3) Semi-major axis of the aperture used for the $R - K$ color, i.e., the 2MASSX isophote where $K = 20$ mag arcsec^{-2}. (4) R-band apparent magnitude in the 2MASSX K20 aperture, with masking to match 2MASSX, uncertainty 0.05 mag. (5) and (6) $R - K$ color, both bands measured in the same aperture. Column 6 is converted to rest frame. (7) 2MASS $J - K$ color, converted to rest frame. (8) Semi-major axis of the isophote at 22.5 mag arcsec^{-2}.
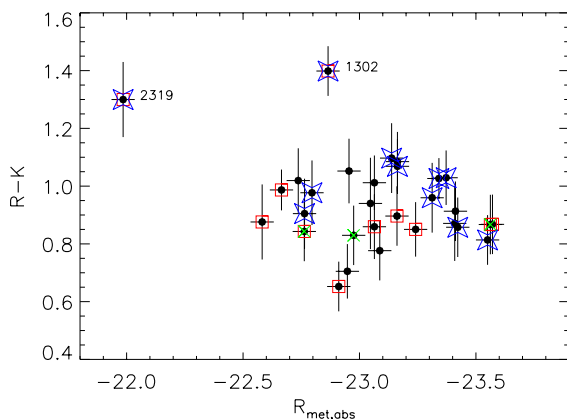

Figure 3. BCG color vs. absolute metric magnitude in AB units, rest frame, corrected for Galactic dust extinction. Symbols indicate special sub-samples: cooling time less than 2 Gyr (blue star), disturbed X-ray emission (red square), and large separation between BCG and X-ray peak (green X). In general, the BCGs have similar color and no dependence of color on magnitude; the exceptions are RXCJ1302 and RXCJ2319, see Section 5.

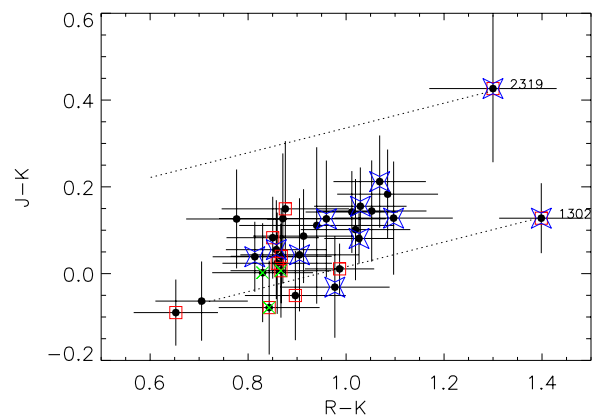(A color version of this figure is available in the online journal.)

Figure 4. BCG colors in AB units, rest frame, corrected for Galactic dust extinction. Symbols same as Figure 3. The dotted lines indicate reddening due to dust internal to the BCG; the length of the line indicates extinction from $A_V = 0$ to 1 for the outliers RXCJ1302 and RXCJ2319, see Section 5.

(A color version of this figure is available in the online journal.)

extinction corrections of Schlegel et al. (1998) as implemented in the calculator at the NASA Extragalactic Database; correc-

tions ranged from 0.04 to 0.40 mag. We converted the magnitudes to rest frame using the *kcorrect* software (Blanton & Roweis 2007), assuming a non-evolving Luminous Red Galaxy
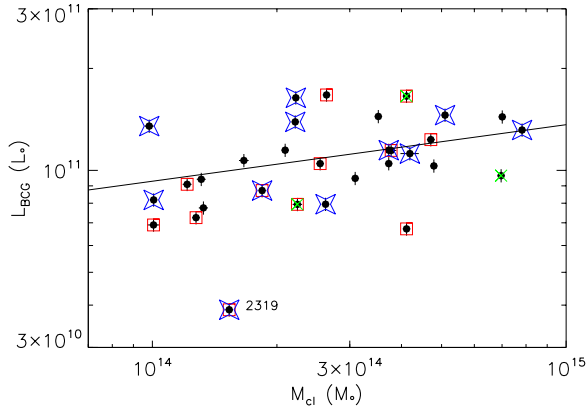
Figure 5. BCG metric luminosity (radius $12\,h^{-1}$ kpc) depends slightly on total cluster mass. Symbols same as Figure 3. The line shows the BCES(Y|X) fit to the data (excluding RXCJ2319, see Section 5) with a power law of 0.18 ± 0.07.

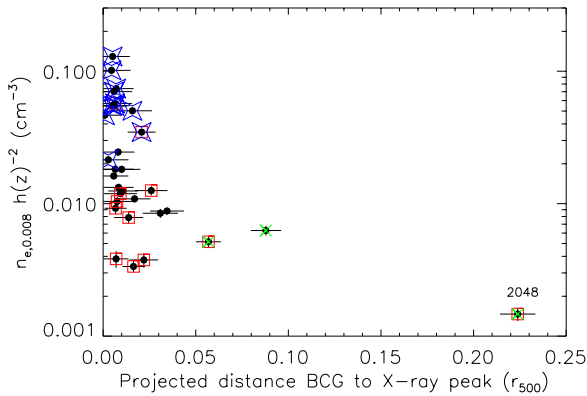(A color version of this figure is available in the online journal.)

Figure 6. In CC clusters, the BCG is co-located with the peak of the X-ray emission; 90% of BCGs in the sample are located within $0.035\,r_{500}$. Symbols same as Figure 3.

(A color version of this figure is available in the online journal.)

Figure 7. Gas density of the cluster at $0.008\,r_{500}$ vs. the BCG metric luminosity (effectively the stellar mass density inside a radius of $12\,h^{-1}$ kpc). Symbols same as Figure 3. The line is a BCES (orthogonal) fit to the non-CC population (excluding RXCJ2048, see Section 5), with a power law of 2.7 ± 0.4.

(A color version of this figure is available in the online journal.)

Figure 8. Gas density of the cluster at $0.008\,r_{500}$ vs. the total cluster mass. Symbols same as Figure 3. There is no correlation between the core gas density and the overall cluster mass.

(A color version of this figure is available in the online journal.)

spectral template; corrections range from 0.05 to 0.18 mag. In Tables 3 and 4 we list magnitudes and colors with and without k-corrections so workers may apply their own spectral energy distribution (SED) and star formation history.

3.5. Colors

BCGs typically have similar colors because they have old stellar populations. To confirm this, we measured $R - K$ colors for the sample, making use of the Two Micron All Sky Survey Extended Source Catalog (2MASSX; Skrutskie et al. 2006). In 2MASSX, the recommended catalog magnitudes (K_{k20fe}) are isophotal ($K = 20$ mag arcsec^{-2} with typical radii 10–50 kpc) inside an elliptical aperture with bright neighbors masked out. To determine accurate colors, however, both bands must be measured in the same aperture with the same objects masked. We could either use the R-band mask and ellipses (Section 3.4) on the 2MASS image (giving a K to match $R_{\rm met}$), or use the 2MASSX mask and ellipses on the R-band image (giving an R_{K20} to match K_{k20fe}). We used the latter method because of the difference in pixel scale between SOAR and 2MASS ($0\rlap{.}{''}154$ versus $1''$). If the precise SOAR masks were applied to the low resolution 2MASSX image, many more pixels of BCG light would be masked, leaving few pixels for the ellipse fit. Instead, we masked the same objects in the SOAR image as were masked in 2MASSX and fixed the central coordinates, ellipticity, and
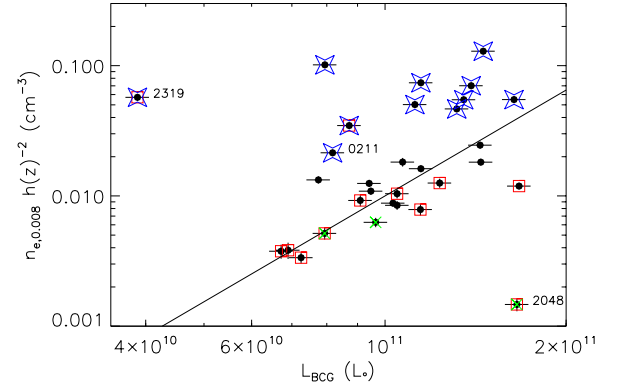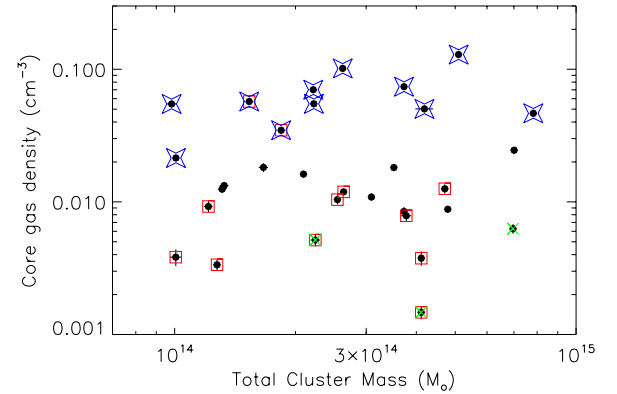
position angle to the 2MASSX values during the ellipse fits. We then proceeded with integration as in Section 3.4. The resulting R_{K20} values and $R - K$ colors are listed in Table 4.

Figures 3 and 4 show the $R - K$ colors as they depend on absolute magnitude and on the $J - K$ color from 2MASSX. With the exception of RXCJ1302 and RXCJ2319 (see Section 5), the colors have very little scatter and no trend with absolute magnitude. This consistency demonstrates that our methods have not introduced significant systematic errors relative to the 2MASS photometry.

4. CORRELATION OF BCG AND GAS PROPERTIES

4.1. Cluster Mass versus BCG Mass

Hierarchical formation models suggest that the mass of the BCG should be correlated with the mass of its host cluster. For example, Whiley et al. (2008) recently calculated the expected dependence, using the models of De Lucia & Blaizot (2007), to be $M_{\rm BCG} \propto M_{\rm cl}^{0.4}$ or $M_{\rm cl}^{0.5}$ depending on the feedback model used. A correlation between BCG luminosity and cluster X-ray luminosity has long been noted in the literature (e.g., Schombert 1988; Edge 1991; Edge & Stewart 1991; Hudson & Ebeling 1997). Here we give an overview of recent results, which tend toward a shallower power-law dependence than predicted by models. For example, Whiley et al. (2008) measured the

Table 5
Correlation Statistics

Parameters	CC Clusters		Non-CC Clusters		All Clusters	
	R	P	R	P	R	P
Optical–Optical						
$R - K$ vs. L_{BCG}	0.41	0.24	0.12	0.64	0.13	0.49
$R - K$ vs. $J - K$	0.73	0.016	0.70	0.00078	0.70	0.000020
X-ray–X-ray						
n_e vs. M_{cl}	0.37	0.29	0.095	0.70	0.067	0.73
n_e vs. $\langle w \rangle$	0.33	0.35	−0.74	0.00026	−0.56	0.0017
X-ray–Optical						
M_{cl} vs. L_{BCG}	0.16	0.65	0.46	0.047	0.38	0.040
n_e vs. e	−0.091	0.80	−0.067	0.78	−0.26	0.17
$\langle w \rangle$ vs. L_{BCG}	−0.37	0.29	−0.44	0.060	−0.46	0.012
n_e vs. L_{BCG}	0.36	0.31	0.67	0.0016	0.56	0.0017

Notes. R is the Spearman rank-order correlation coefficient. P is the probability that the parameters are not correlated. Correlations with the offset between the BCG and X-ray peak are not listed because many offsets are consistent with zero. Clusters RXCJ2319 and RXCJ2048 have been left out of all statistics, see Section 5.

correlation as $M_{\mathrm{BCG}} \propto M_{\mathrm{cl}}^{0.12\pm0.03}$ for K-band magnitudes inside a diameter of 37 kpc (radius of $13\,h^{-1}$ kpc). Brough et al. (2008) saw a similar dependence of $L_{\mathrm{BCG}} \propto M_{\mathrm{cl}}^{0.11\pm0.10}$ at K band inside $12\,h^{-1}$ kpc. Yang et al. (2008) found $L_{\mathrm{BCG}} \propto M_{\mathrm{cl}}^{0.17}$ for galaxy groups. Lin & Mohr (2004) found a steeper dependence ($L_{\mathrm{BCG}} \propto M_{\mathrm{cl}}^{0.26\pm0.04}$), but they used isophotal magnitudes rather than metric magnitudes. (Isophotal magnitudes favor larger, more massive galaxies; in terms of Figure 2, isophotal magnitudes make a horizontal cut through the profiles while metric magnitudes make a vertical cut.) Similarly, Popesso et al. (2007) found $L_{\mathrm{BCG}} \propto M_{\mathrm{cl}}^{0.25}$ using r-band Petrosion magnitudes. Stott et al. (2008) used K-band isophotal magnitudes and found an even steeper relation (-1.1 ± 0.3 mag per decade of X-ray luminosity, or $L_{\mathrm{BCG}} \propto L_{\mathrm{cl}}^{0.44\pm0.12}$) when fitting only to clusters with high X-ray luminosity. Mittal et al. (2009) used K-band total magnitudes (extrapolating the Sersic profile) and found $L_{\mathrm{BCG}} \propto M_{\mathrm{cl}}^{0.62\pm0.05}$; they note that total magnitudes give a stronger correlation with cluster properties than smaller aperture magnitudes.

For our sample, we measured L_{BCG} in R band inside $12\,h^{-1}$ kpc. We confirm the weak trend between BCG luminosity and cluster mass. Figure 5 shows the trend, which has substantial scatter; Table 5 shows that the correlation is marginally significant. Unlike Stott et al. (2008), we do not see the trend becoming more prominent at higher X-ray luminosities. Fitting in log–log space using the bivariate correlated errors and intrinsic scatter (BCES(Y|X)) regression method (Akritas & Bershady 1996), we find $L_{\mathrm{BCG}} \propto M_{\mathrm{cl}}^{0.18\pm0.07}$, consistent with the results found by others using metric magnitudes.

4.2. Core Gas Density versus BCG Ellipticity

We noticed a possible correlation between core gas density and BCG ellipticity. Neglecting RXCJ2319 (see Section 5), the largest ellipticity among the CC clusters is 0.29. The largest ellipticity among the non-CC clusters is 0.53, and half of the non-CC clusters have ellipticities larger than 0.29. This comparison suggests that BCGs in CC clusters are rounder than those in non-CC clusters. A K-S test shows that this trend is not

statistically significant for the small numbers of our sample, so a larger sample is needed to test the trend suggested by these data.

4.3. Core Gas Density versus BCG Location

The offset between the X-ray peak and the BCG position is listed in Table 1 and plotted in Figure 6. The *XMM-Newton* resolution prevents a precise measure of this offset at the smallest separations, but *XMM-Newton* can clearly identify clusters where the BCG is located far from the X-ray peak. We find that three BCGs are located more than $0.035\,r_{500}$ (and more than $30''$) from the X-ray peak, all of which have multiple galaxies of similar brightness. That leaves 28/31 (90%) of the clusters with a galaxy closer than $0.035\,r_{500}$. Note that the REXCESS sample is unbiased with respect to X-ray morphology, so this close agreement is not due to an overrepresentation of bright X-ray cores in the sample.

Our high fraction of small offsets (90%) is higher than Lin & Mohr (2004) found in a sample of 93 clusters: ∼65% within the same radius ($0.02R_{200}$ in their Figure 1). The difference from our results is likely because their sample is infrared selected, has X-ray data drawn from several catalogs, and uses X-ray peak positions from lower resolution *ROSAT* data.

We also found more small offsets than Loubser et al. (2009) found in a sample of 49 BCGs. They found 45% of BCGs falling within 20 kpc of the X-ray peak while we find 77% within that distance. This difference is likely due to different sample selection and to their exclusion of galaxies that fall near the peak if the peak is far from the literature X-ray position (their Table 7).

Our sample is more comparable to that of Sanderson et al. (2009), who studied the LoCUSS sample of 65 X-ray-selected clusters. They found 75% of BCGs falling within $0.04\,r_{500}$ of the X-ray centroid, while we found 90% within that distance of the X-ray peak. These percentages are consistent given Poisson statistics.

Our results agree with Hudson et al. (2009), who study 64 clusters in the HIFLUGCS sample. They found 88% to have a BCG within $50\,h^{-1}$ kpc of the X-ray peak, while we find 90% within that radius.

Recent work by Bildfell et al. (2008), Rafferty et al. (2008), and Sanderson et al. (2009) found that star formation in CCs requires that the X-ray and galaxy centroids lie within ∼20 kpc of each other. Our data agree; all 11 CC clusters have offsets less than 20 kpc, while 13 out of 20 non-CC have such small offsets. Like Sanderson et al. (2009), we find that steep central X-ray profiles have small BCG offsets, similar to the correlation between central gas density with BCG offset shown in Figure 6.

Bildfell et al. (2008) find a correlation between BCG absolute B-band magnitude and the offset from the X-ray peak, where BCGs are fainter when located far (up to 500 kpc) from X-ray peak. We see no such correlation at large offsets in R band.

4.4. Gas Dynamical State versus BCG Location

We noticed a possible correlation between large values of $\langle w \rangle$ (indicating disturbed gas) and large offset between the BCG and the X-ray peak. RXCJ2048 and RXCJ2129 are two of the three most disturbed clusters (the other is RXCJ2157), and are also two of the three largest BCG offsets (the other is RXCJ2234). The correlation is difficult to quantify for small offsets, since many of our measured offsets are consistent with zero. The correlation for large offsets is not surprising: clusters

with disturbed gas have likely undergone recent mergers and the largest galaxies have not had time to settle into the core.

4.5. Core Gas Density versus BCG Central Stellar Density in Non-CC Clusters

4.5.1. Observed Trend

We compared several optical properties of BCGs with various X-ray properties of the intracluster gas, and in most cases we saw little or no correlation. (Some of these are reported in Table 5 and describe above.) The tightest correlation, however, between X-ray and optical properties was one we did not expect: between the core gas density of non-CC clusters and their aperture BCG luminosity, shown in Figure 7.

The correlation appears to follow a power law, with outliers mainly toward higher core gas density. The rank order correlation statistics are reported in Table 5: for the non-CC sample (excluding RXCJ0211 and RXCJ2048; see Section 5), the parameters show less than 0.16% chance of being uncorrelated, a detection stronger than 3σ. A BCES (orthogonal) fit in log–log space finds $n_e \propto L_{BCG}^{2.7\pm0.4}$. We also note that the correlation cannot be a spurious effect of the X-ray point spread function, since non-CC clusters have broad, flat centers that are well resolved by *XMM-Newton*.

Note that the correlation is with aperture luminosity, not total luminosity. The aperture luminosity is proportional to the mass in the inner $12\,h^{-1}$ kpc, and so is a good proxy for the central stellar mass density of the galaxy (it is not a good proxy for the total mass of the galaxy). When discussing this trend, we will refer to L_{BCG} as central stellar density. Thus, we discovered that, for non-CC clusters, the BCG central stellar density is larger in clusters with larger core gas densities. We tested the correlation using several measures of BCG luminosity, but found that well-masked metric magnitudes give the tightest correlation (Table 5 shows $P = 0.0016$). Well-masked isophotal magnitudes in R band also showed some correlation ($P = 0.015$), but K_{k20fe} isophotal magnitudes from 2MASSX showed little correlation ($P = 0.14$). 2MASSX reports magnitudes with some bright objects masked, but not as completely masked as we could do with deeper, better-sampled images in R band.

We tested whether other related parameters would show the relationship more clearly, but found that core gas density and BCG metric luminosity had the strongest correlation (Table 5). In place of BCG metric luminosity, we tried metric surface brightness. In place of core gas density, we tried cooling time and centroid shift. In no case was the correlation as tight as the one shown. Croston et al. (2008) reported the correlation of n_e with X-ray centroid shift $\langle w \rangle$ (in opposing directions for the CC and non-CC samples), which in turn introduces a correlation of L_{BCG} with $\langle w \rangle$, but this is not as tight as L_{BCG} with n_e. We tested if the correlation of n_e and L_{BCG} could be tightened further by removing any additional dependence on $\langle w \rangle$, but saw little improvement.

We note that the correlation is driven by a population of five clusters with the lowest core gas densities: RXCJ0145, 0225, 2129, 2157, 2234. These five have not only the lowest core gas density, but are also the only clusters with multiple galaxies of similar brightness (which we classify as type 3). Three of the clusters (RXCJ0145, 2129, 2157) are among the most disturbed clusters in the sample. All three indicators suggest a young dynamic age, so this subsample points to cluster dynamics as key to the interpretation of the relation.

4.5.2. Interpretation

What could be the physical cause of this correlation? In no way do we suggest that the ICM gas density has a *direct* effect on the stars of the BCG; that would be unphysical. Rather, the explanation of the correlation must be based in some other physical process that affects both the core gas density and the central stellar density. What processes could be involved?

BCGs and core gas are known to be related via the stars that form from the cooling gas. This causes BCGs in CC clusters to show more indicators of star formation than BCGs in non-CC clusters, including Hα emission (e.g., Cavagnolo et al. 2008), blue color (e.g., Bildfell et al. 2008), and younger stellar populations (e.g., Loubser et al. 2009). Similar studies are being done for the REXCESS sample (Donahue et al. 2010, submitted). Our correlation, however, is seen in R band, which detects the mass of the old stellar population, not recent star formation.

In fact, it seems unlikely that this old stellar population should be correlated with the presence or absence of a CC, since the CC gas and the stars have such different time scales. Prominent CCs have radiative cooling times shorter than a billion years, whereas the vast majority of the stars formed several billion years ago, based on studies of their color–magnitude relation and SEDs at $z \sim 1$ (e.g., Andreon et al. 2008; Stott et al. 2008). Collins et al. (2009) suggest that even the assembly of BCGs is mostly complete before redshift 1.

For these reasons, the correlation is not explained by the relationship between strong CCs and star formation. Moreover, the correlation is in the non-CC population, not the CC population. In non-CC clusters, the gas is much too diffuse to cool and form stars. Some process other than star formation must be at work.

The correlation is not due to overall cluster properties, such as total mass, X-ray luminosity, or gas temperature. It is not the case that more massive clusters simply have more luminous BCGs and denser core gas. While the BCG central stellar density does depend weakly on total mass (Figure 5) with a power of 0.18 ± 0.07, that trend cannot solely explain the much stronger dependence (power of 2.7 ± 0.4) on core gas density. Moreover, the core gas density has no correlation with system temperature (Croston et al. 2008) or with total cluster mass (Figure 8, Table 5).

The correlation is not primarily due to the BCG gravitational potential. It is true that the BCG is located near the X-ray peak in most cases (Figure 6), and that a larger stellar density would increase the gravitational potential well. If this were the sole cause, however, the core gas density would be expected to be only modestly dependent on the central stellar density, but the observed relationship has a power of 2.7. In addition, two clusters with BCGs located far from the X-ray core also fall on the trend, implying that physical proximity is not required.

The correlation might be due to a few clusters that have experienced a recent merger. As noted above, the five clusters with lowest gas density include the three clusters with the most disturbed gas, suggesting a recent merger (Table 5 shows the strong correlation of gas density and $\langle w \rangle$ in non-CC clusters). These five clusters also have multiple galaxies of similar brightness rather than a single dominant BCG, as expected for a recent cluster merger where the central galaxies have not yet merged into one BCG. After the merger, the resulting BCG would have higher total luminosity, but before the merger there is a time window when the gas density is low and the BCG total luminosity is low. This sounds like a promising explanation of the trend, but there is a problem. The L_{BCG} we report is a metric

aperture luminosity in $12\,h^{-1}$ kpc, not a total luminosity; as noted above, it is a better proxy for central stellar density than for total mass. How is central stellar density affected by a merger? Mergers between ellipticals are known to decrease the central density cusp, producing the well-known trend of lower central surface brightness in higher luminosity elliptical galaxies. Thus, the galaxies corresponding to low gas density are those with low stellar densities, which would be *after* their mergers rather than the cuspy galaxies seen in the window between gas merger and galaxy merger.

We suggest that mergers are key to the explanation, but that it is the long-term merger history of the cluster rather than the most recent merger. Mergers of sub-clusters cause gas shocks which increase the gas entropy. More massive clusters have larger shocks and thus larger entropy gains. In the absence of galaxies and feedback, models show that the final entropy profile of the gas is determined by total cluster mass, leading to a self-similar family of entropy profiles (reviewed in Voit 2005). The entropy at the core, however, tends to deviate from the self-similar relation.

The core gas density can serve as a proxy for the deviation of the core entropy relative to other clusters of the same mass. In a self-similar cluster model, the ratio of core entropy K_0 to the entropy K_Δ at some large scale radius r_Δ is

$$\frac{K_0}{K_\Delta} = \left(\frac{T_0}{n_0^{2/3}}\right)\left(\frac{n_\Delta^{2/3}}{T_\Delta}\right).$$

The gas density n_Δ at r_Δ is the same for all clusters by definition. The ratio T_0/T_Δ can be affected by non-gravitational processes but is closely tied to gravitational potential, so T_0/T_Δ is not observed to vary much across self-similar clusters. Thus, in practice, the expression reduces to

$$\frac{K_0}{K_\Delta} \propto n_0^{-2/3}.$$

In other words, the central gas density is closely related to the relative enhancement of central entropy over what would be expected in a self-similar cluster, independent of cluster mass. A cluster whose central entropy was unusually large for its halo mass would therefore have an unusually low central density.

Many physical processes can change the core entropy level, including radiative cooling, supernova or AGN feedback, and conduction. What we have discovered here is that, whatever the process, it also appears to set the central stellar density of the BCG. While most processes that affect gas entropy have little effect on stars, mergers affect both. The details of the merger history, such as the size of the sub-clusters, may be the cause of these deviations from the self-similar value. As stated above, mergers also affect stellar density, decreasing the cusp and reducing the central stellar density. Thus, mergers could increase gas entropy, decrease gas density, and decrease stellar density. In this way, the central stellar density would provide a record of the merger history of the cluster. The core gas in non-CC clusters has a very long cooling time and does not experience feedback, so it too preserves a memory of the shocks experienced in the merger history. In our sample, even disturbed clusters (red squares on the figures) fall on the trend, suggesting that the correlation is dominated by long-term merger history, not recent merger events.

The CC sample does not follow a similar power-law trend. In these clusters, radiative cooling and feedback have a greater influence on the core gas, allowing the entropy to decrease and

the gas density to increase beyond the level set by mergers. This increase does not have a particular correlation with BCG stellar density. The outliers on the upper side of the non-CC trend may be in transition to higher gas density via these processes.

5. SPECIAL CASES

RXCJ0211. This cluster is classified by Pratt et al. (2009) as non-CC based on its central gas density and central cooling time, but we classify it as CC based on its cooling time at 0.03 r_{500} (see Section 2). It has the lowest gas temperature of all the clusters in REXCESS, giving it a shorter cooling time than other clusters of similar gas density such as RXCJ0645. Like all CC clusters in REXCESS, it hosts a central radio source, something that some non-CC clusters lack (a full analysis of REXCESS radio properties will appear in S. Heidenreich et al. 2010, in preparation). If RXCJ0211 is instead put in the non-CC sample, the trend between core gas density and BCG stellar density (Figure 7, Section 4.5.1) is still present but a bit less significant ($R = 0.57$, $P = 0.01$).

RXCJ0049 and RXCJ0225. In these clusters, the galaxy located at the X-ray peak is in the 2MASS Point Source catalog but not in the 2MASSX extended source catalog. Thus, we did not have the K-band profile parameters needed to measure the $R - K$ color using the method in Section 3.5.

RXCJ1302. This galaxy has a redder $R - K$ color than the rest of the BCGs in the sample (Figure 3). Yet its $R_{\mathrm{met,abs}}$ magnitude (Figure 3) and $J - K$ color (Figure 4) are consistent with the rest of the sample. One possible explanation is dust internal to the galaxy (found in other BCGs in CC clusters, e.g., Egami et al. 2006; O'Dea et al. 2008). Assuming a typical extinction curve (Gordon et al. 2003), about 0.5 mag of internal extinction in $R_{\mathrm{abs,met}}$ would bring the $R - K$ color in line with the rest of the sample while keeping $J - K$ consistent with the sample. If such a change is made, the power fit in Figure 5 would change only slightly to 0.17 ± 0.07. The fit in Figure 7 is unaffected because this cluster is not in the non-CC sample.

RXCJ2048. This cluster is an outlier in the lower left of Figure 7. Of the clusters in the sample, it has the largest separation between the BCG position and X-ray peak (Figure 6). The BCG may be misidentified, although the only other candidate in the field is slightly fainter and located just as far from the X-ray peak on the opposite side of the X-ray centroid. Its X-ray properties are unique as well, having the most diffuse X-ray emission (Figure 1) and the longest cooling time (Table 1) of the entire sample. It is possible that the gas is not even in hydrostatic equilibrium. Because of these multiple issues, we leave it out of the fit in Figure 7 and out of the statistics in Table 5.

RXCJ2319. This galaxy has a much fainter absolute magnitude than the rest of the BCGs in the sample (Table 3). We reobserved the galaxy on another night and confirmed the faint R magnitude. A misidentification is unlikely, since the galaxy is clearly the brightest in the field and coincident with the X-ray peak. A faint magnitude and red color could be caused by an incorrect redshift, but the optical redshift $z = 0.0984$ from Guzzo et al. (2009) is confirmed by our own observations of faint emission lines in the BCG at $z = 0.0979$ (Donahue et al. 2010, submitted). In addition, its $R - K$ and $J - K$ colors are extremely red (Figures 3, 4), while its $J - H$ color from 2MASSX is consistent with the sample. That suggests an excess of K emission, perhaps similar to the obscured Seyfert BCG in Abell 1068 (Edge et al. 2002), except the optical spectrum shows very typical line widths rather than the strong lines of AGN activity. Thus, we do not have a good explanation for this object,

but because of its puzzling nature we leave it out of the fits in Figures 5 and 7 and out of the statistics in Table 5.

6. SUMMARY

Using the REXCESS sample of galaxy clusters, we investigated the relationships between the BCG stellar mass and the properties of the X-ray emitting gas. We confirmed the weak correlation seen by others between the BCG luminosity and the total cluster mass, and the close proximity of the BCG to the X-ray peak.

We detected a trend among the non-CC clusters in which the core gas density increases with the BCG aperture luminosity, a proxy for the BCG central stellar mass density. This trend is much clearer when the BCG luminosity is determined from well-masked aperture magnitudes rather than from unmasked or isophotal magnitudes. This trend holds even in cases where the gas is disturbed or the BCG is located far from the central region. We argue that the core gas density is an indicator of the deviation of the central entropy from the self-similar value. Thus, the core gas entropy and the central BCG stellar density appear to be more closely related than previously thought. We suggest that cluster mergers could be the underlying cause, since mergers can both increase gas entropy and decrease BCG central stellar density. If so, this trend could set important constraints on models of the central gas in clusters and of BCG formation.

These results are based on a sample of only 31 clusters, and need to be confirmed using other, larger cluster samples. For example, Cavagnolo et al. (2009) recently fit entropy profiles to 239 clusters from the *Chandra* X-ray Observatory archive. The optical data corresponding to this or other large samples of X-ray-selected clusters would allow an investigation of the trend with a statistically significant sample size. If the trend is real and our interpretation is correct, it should be present independent of how the clusters are selected.

REFERENCES

Adelman-McCarthy, J., et al. 2008, ApJS, 175, 297
Akritas, M. G., & Bershady, M. A. 1996, ApJ, 470, 706
Andreon, S., Puddu, E., de Propris, R., & Cuillandre, J.-C. 2008, MNRAS, 385, 979
Arnaud, M., Pointecouteau, E., & Pratt, G. W. 2007, A&A, 474, L37
Bildfell, C., Hoekstra, H., Babul, A., & Mahdavi, A. 2008, MNRAS, 398, 1637
Blanton, M. R., & Roweis, S. 2007, AJ, 133, 734
Böhringer, H., et al. 2001, Messenger, 106, 24
Böhringer, H., et al. 2007, A&A, 469, 363
Böhringer, H., et al. 2009, A&A, submitted (arXiv:0912.4667)
Brough, S., Couch, W. J., Collins, C. A., Jarrett, T., Burke, D. J., & Mann, R. G. 2008, MNRAS, 385, L103
Cavagnolo, K., Donahue, M., Voit, G. M., & Sun, M. 2008, ApJ, 683, L107
Cavagnolo, K., Donahue, M., Voit, G. M., & Sun, M. 2009, ApJ, 182, 12
Clemens, J. C., Crain, J. A., & Anderson, R. 2004, Proc. SPIE, 5492, 331
Collins, C. A., et al. 2009, Nature, 458, 603
Croston, J. H., Arnaud, M., Pointecouteau, E., & Pratt, G. W. 2006, A&A, 456, 1007
Croston, J. H., et al. 2008, A&A, 487, 431
De Lucia, G., & Blaizot, J. 2007, MNRAS, 375, 2
Donahue, M., & Voit, G. M. 2004, in Clusters of Galaxies: Probes of Cosmological Structure and Galaxy Evolution, ed. J. S. Mulchaey, A. Dressler, & A. Oemler (Cambridge: Cambridge Univ. Press), 143
Donahue, M., et al. 2010, ApJ, submitted
Edge, A. C. 1991, MNRAS, 250, 103
Edge, A. C., & Stewart, G. C. 1991, MNRAS, 252, 428
Edge, A. C., Wilman, R. J., Johnstone, R. M., Crawford, C. S., Fabian, A. C., & Allen, S. W. 2002, MNRAS, 337, 49
Egami, E., et al. 2006, ApJ, 647, 922
Gordon, K. D., Clayton, G. C., Misselt, K. A., Landolt, A. U., & Wolff, M. J. 2003, ApJ, 594, 279
Guzzo, L., et al. 2009, A&A, 499, 357
Hamuy, M., Walker, A. R., Suntzeff, N. B., Gigoux, P., Heathcote, S. R., & Phillips, M. M. 1992, PASP, 104, 533
Hausman, M. A., & Ostriker, J. P. 1978, ApJ, 224, 320
Hudson, D. S., Mittal, R., Reiprich, T. H., Nulsen, P. E. J., Andernach, H., & Sarazin, C. L. 2009, A&A, in press (arXiv:0911.0409)
Hudson, M. J., & Ebeling, H. 1997, ApJ, 479, 621
Jones, C., & Forman, W. 1984, ApJ, 276, 38
Kay, S. T., da Silva, A. C., Aghanim, N., Blanchard, A., Liddle, A. R., Puget, J.-L., Sadat, R., & Thomas, P. A. 2007, MNRAS, 377, 317
Landolt, A. U. 1992, AJ, 104, 340
Lin, Y.-T., & Mohr, J. J. 2004, ApJ, 617, 879
Loubser, S. I., Sánchez-Blázquez, P., Sansom, A. E., & Soechting, I. K. 2009, MNRAS, 398, 133
McNamara, B. R., & Nulsen, P. E. J. 2007, ARA&A, 45, 117
Mittal, R., Hudson, D. S., Reiprich, T. H., & Clarke, T. 2009, A&A, 501, 835
O'Dea, C. P., et al. 2008, ApJ, 681, 1035
Popesso, P., Biviano, A., Böhringer, H., & Romaniello, M. 2007, A&A, 464, 451
Postman, M., & Lauer, T. R. 1995, ApJ, 440, 28
Pratt, G. W., Böhringer, H., Croston, J. H., Arnaud, M., Borgani, S., Finoguenov, A., & Temple, R. F. 2007, A&A, 461, 71
Pratt, G. W., Croston, J. H., Arnaud, M., & Böhringer, H. 2009, A&A, 498, 361
Rafferty, D. A., McNamara, B. R., & Nulsen, P. E. J. 2008, ApJ, 687, 899
Sanderson, A. J. R., Edge, A. C., & Smith, G. P. 2009, MNRAS, 398, 1698
Schlegel, D. J., Finkbeiner, D. P., & Davis, M. 1998, ApJ, 500, 525
Schombert, J. M. 1988, ApJ, 328, 475
Schwarz, H. E., et al. 2004, Proc. SPIE, 5492, 564
Skrutskie, M. F., et al. 2006, AJ, 131, 1163
Stott, J. P., Edge, A. C., Smith, G. P., Swinbank, A. M., & Ebeling, H. 2008, MNRAS, 384, 1502
Vale, A., & Ostriker, J. P. 2008, MNRAS, 383, 355
Voit, G. M. 2005, Rev. Mod. Phys., 77, 207
Walker, A. R., et al. 2003, Proc. SPIE, 4841, 286
Whiley, I. M., et al. 2008, MNRAS, 387, 1253
Yang, X., Mo, H. J., & van den Bosch, F. C. 2008, ApJ, 676, 248